14th World Congress on Computational Mechanics (WCCM)
ECCOMAS Congress 2020)
Virtual Congress: 11-–15 January 2021
F. Chinesta, R. Abgrall, O. Allix and M. Kaliske (Eds)

ON THE THERMODYNAMICS OF DYNAMIC RECRYSTALLIZATION FOR VISCOPLASTICITY AT LARGE STRAINS

Hendrik Westermann[1], **Rolf Mahnken**[1]

[1] Chair of Engineering Mechanics, Paderborn University
Warburger Straße, 33098 Paderborn, Germany
westermann@ltm.upb.de
www.upb.de/person/60816

Key words: thermodynamic framework, dynamic recrystallization, viscoplasticity, dislocation density, large strains

Abstract. During the thermo-mechanical processing of metals, complex microstructure evolution inevitably occur, altering the marcoscopic material properties. The vital microstructure mechanisms include viscoplastic deformation, dynamic recovery (DRV) and dynamic recrystallization (DRX), leading to the hardening and softening of the material. A thermodynamic framework for dynamic recrystallization is proposed covering the state in crystalline materials. Several improvements are presented for an internal state variable (ISV) model to consider the evolution of dislocations dependent on recrystallized volume fractions and derive the constitutive relations for microscopic and macroscopic quantities coupled to viscoplasticity. The relation between microscopic quantities and the macroscopic hardening stress is clarified based on thermodynamic arguments and thermodynamic consistency is derived. On the numerical side a suitable explicit/implicit algorithm is presented and the evolution equations are validated based on experimental data for OFHC copper. During parameter identification the material parameters are determined solving the inverse problem. In numerical examples the constitutive equations are applied to simulations for uniaxial loading and the characteristics of continuous dynamic recrystallization such as strain softening are illustrated.

1 INTRODUCTION

Complex microstructure mechanisms, such as dynamic recovery and dynamic recrystallization heavily affect material properties in engineering alloys. During hot deformation dislocation evolution changes the material properties on the macroscopic scale. The prediction of microstructure mechanisms during the hot forming of alloys leads to the adjustment of microstructures and thus to the gradation of mechanical properties.

The focus lies on the mechanism of dynamic recrystallization. It describes the formation of strain free grains and their successive growth until the stored energy of the initial deformed microstructure is consumed. The grain boundary motion sweeps away the build-up dislocation structure, thus reducing the dislocation density. During the process two phases are distinguished. According to [1] the material consists of a hard unrecrystallized phase and a soft recrystallized phase. During plastic deformation the dislocation density increases in the unrecrystallized phase leading to the harding of the material. In the recrystallized phase the dislocations are annihilated and sub grain boundaries are removed by dynamic recrystallization. During the process of dynamic recrystallization, the recrystallized and unrecrystallized phases harden and recover with plastic deformation, thus recrystallizing in cycles resulting in multi-peak

behavior.

In the present paper the continuum mechanical model for dynamic recrystallization in [2] is considered as a point of departure for further investigations. It is based on the internal state variable framework proposed in [3] which was further developed in [4], [5] and [6]. The model in [2] combines a phenomenological viscoplastic model with microstructural internal state variables representing dislocation densities.

Though conceptionally well advanced, the following aspects of the works on on dynamic recrystallization are worthwhile being improved: In [2] the microscopic stresses in the unrecrystallized phase are assumed (rather than derived) to evolve unaltered by the recrystallization process. In the plastic potential for the macroscopic hardening stress, simply a sum of microscopic internal stress like variables is assumed to represent the macroscopic yield stress without any further justification.

The general idea of the present work is to close the aforementioned gaps in [2]. The key objective is to provide a general thermodynamic framework accounting for the microstructural mechanism of dynamic recrystallization. Regarding the physical mechanism, the internal state variable model provided by [2] is reworked to include recrystallization volume fractions at the onset of the thermodynamic framework and to derive the constitutive relation for macroscopic and microscopic quantities in recrystallized media in accordance with thermodynamic arguments.

2 THERMODYNAMIC FRAMEWORK

The following thermodynamic framework distinguishes between the macroscopic scale and the microscopic scale. The scales of the two-scale model are illustrated in Figure 1.

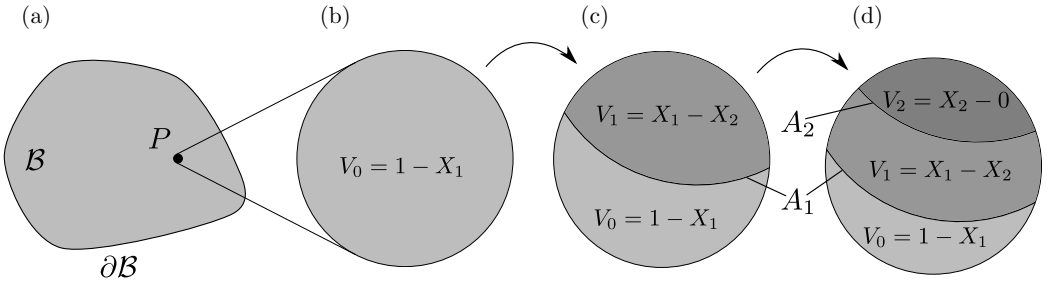

Figure 1: Two-scale model: (a) Macroscopic scale with material point P, (b)-(d) microscopic scale with interfacial areas A_i between volume fractions V_i of recrystallized regions for two recrystallization cycles.

2.1 Kinematics

The thermodynamic framework of the current proposal is set within the theory of large strains. At each material point P of a macroscopic body $\mathcal{B}$ in Figure 1 the deformation gradient $\mathbf{F}$ and its Jacobian J is introduced. This maps the line segments $d\mathbf{X}$, volume elements dV and area elements $d\mathbf{A}$ of the reference configuration $\mathcal{B}_0$ to its corresponding quantities of the current configuration $\mathcal{B}$:

$$1. \quad d\mathbf{x} = F \cdot d\mathbf{X}, \quad 2. \quad dv = JdV, \quad 3. \quad J = \det\mathbf{F}. \tag{1}$$

The macroscopic kinematics are based on a multiplicative split of the deformation gradient

$$1.\quad \mathbf{F}=\mathbf{F}^{vol}\cdot\mathbf{F}^{iso}=\mathbf{F}^{iso}\cdot\mathbf{F}^{vol}\qquad\Longleftrightarrow\qquad 2.\quad \mathbf{F}^{vol}=J^{1/3}\mathbf{1},\qquad 3.\quad \mathbf{F}^{iso}=J^{-1/3}\mathbf{F}, \tag{2}$$

where $\mathbf{F}^{iso}$ and $\mathbf{F}^{vol}$ are the isochoric and volumetric deformations and $\mathbf{1}$ is the unit tensor of second order. For the modeling of thermo-elasto-viscoplasticity an additional split is required according to [8]. By following the assumptions in [8] we obtain

$$1.\quad \mathbf{F}=\mathbf{F}_e\cdot\mathbf{F}_i\cdot\mathbf{F}_\theta,\qquad \text{where}\qquad 2.\quad \mathbf{F}_e=J_e^{1/3}\mathbf{F}^{iso},\qquad 3.\quad \mathbf{F}_\theta=J_\theta^{1/3}\mathbf{1}. \tag{3}$$

Taking the time derivative of the relation in Eq. (3) the additive decomposition for the velocity gradient with respect to the intermediate configuration renders

$$\begin{aligned}&1.\quad \overline{\mathbf{L}}=\overline{\mathbf{L}}_e+\overline{\mathbf{L}}_i+\overline{\mathbf{L}}_\theta\qquad \text{where}\\ &2.\quad \overline{\mathbf{L}}_e=\mathbf{F}_e^{-1}\cdot\dot{\mathbf{F}}_e,\qquad 3.\quad \overline{\mathbf{L}}_i=\dot{\mathbf{F}}_i\cdot\mathbf{F}_i^{-1}=-\mathbf{F}_i\cdot\dot{\mathbf{F}}_i^{-1},\qquad \overline{\mathbf{L}}_\theta=\mathbf{F}_\theta^{-1}\cdot\dot{\mathbf{F}}_\theta,\end{aligned} \tag{4}$$

with $\overline{\mathbf{L}}_e$, $\overline{\mathbf{L}}_i$ and $\overline{\mathbf{L}}_\theta$ as the elastic, inelastic and thermal part of $\overline{\mathbf{L}}$, respectively. During dynamic recrystallization the material may harden and recover in cycles according to [2]. To capture the multi-peak behavior in recrystallization cycles within the kinematics of the present model, the notation X_i for the recrystallized fraction of the material that went through a minimum of i recrystallization cycles is used. The volume fraction $V_i=X_i-X_{i+1}$ denotes the volume fraction that has recrystallized i times, such that $V_0=1-V_1$ is the unrecrystallized material. Three volume fractions are illustrated schematically in Figure 1 (b)-(d). The volume fraction V_i for the i-th cycle in a general setting renders

$$1.\quad V_i=X_i-X_{i+1},\qquad i=0,\dots,n_c\qquad \text{where}\qquad 2.\quad X_0=1,\qquad 3.\quad X_{n_c+1}, \tag{5}$$

with n_c being the number of recrystallization cycles. Since the evolution of recrystallization quantities does not increase or remove any volume, a completeness condition is required

$$V=\sum_{i=0}^{n_c}V_i=1. \tag{6}$$

Each volume fraction V_i, $i=0,\dots,n_c$ in Figure 1 will have a separate set of internal variables. For the formulation of the internal variables the general representation is

$$1.\quad \Phi_t=\Phi[t,\underline{V}[t]],\qquad 2.\quad \mathring{\Phi}:=\dot{\Phi}+\hat{\Phi},\qquad 3.\quad \dot{\Phi}=\left.\frac{\partial\Phi}{\partial t}\right|_{\underline{V}},\qquad 4.\quad \hat{\Phi}=\left.\frac{\partial\Phi}{\partial\underline{V}}\dot{\underline{V}}\right|_t, \tag{7}$$

valid for any function $\Phi[\cdot,\cdot]$ dependent on time t and volume fraction $\underline{V}$. The total time derivative in Eq. (7) has a convective part $\dfrac{\partial\Phi}{\partial\underline{V}}\dot{\underline{V}}$, to account for time varying recrystallized volume fractions $V_i(t)$. Consequently, for any quantity, which is homogeneously distributed over the RVE it follows

$$1.\quad \Phi_t=\Phi[t],\qquad 2.\quad \hat{\Phi}=\frac{\partial\Phi}{\partial\underline{V}}\dot{\underline{V}}=0\qquad\Longrightarrow\qquad 3.\quad \mathring{\Phi}=\dot{\Phi}. \tag{8}$$

2.2 Balance relations

With respect to the reference configuration $\mathcal{B}_0$ the macroscopic balance relations read

$$\begin{aligned}
&1. \quad \rho_0 \ddot{\mathbf{u}} - \mathrm{Div}\,(\mathbf{F}\cdot\mathbf{S}) && = \rho_0 \mathbf{f}, && \text{(linear momentum)}\\
&2. \quad \rho_0 \dot{e} + \mathrm{Div}\mathbf{q}_0 && = \mathbf{S}:\dot{\mathbf{E}} + \rho_0 r_\theta, && \text{(energy)}\\
&3. \quad -\rho_0 \dot{e} + \rho_0 \theta \dot{\eta} + \mathbf{S}:\dot{\mathbf{E}} - \frac{1}{\theta}\mathbf{q}_0 \cdot \mathrm{Grad}\theta && \geq 0, && \text{(entropy)}
\end{aligned} \tag{9}$$

where ρ_0 is the density (reference configuration), $\mathbf{u}$ is the displacement vector, $\mathbf{S}$ is the second Piola-Kirchhoff stress tensor, $\mathbf{f}$ is the mass of density of external forces, e is the mass density of the internal energy, $\mathbf{q}_0$ is the heat-flux vector, r_θ is the mass density of heat supply and $\mathbf{E} = (1/2)(\mathbf{F}\cdot\mathbf{F})$ ist the Green strain tensor.

With the additive split of the velocity gradient tensor in Eq. (4) the Clausius-Duhem inequality in Eq. (9.3) results in

$$\left(\frac{1}{\rho_0}\overline{\mathbf{M}} - 2\overline{\mathbf{C}}_e \cdot \frac{\partial \Psi}{\partial \overline{\mathbf{C}}_e}\right) : \overline{\mathbf{L}} + 2\overline{\mathbf{C}}_e \cdot \frac{\partial \Psi}{\partial \overline{\mathbf{C}}_e} : \overline{\mathbf{L}}_i - \frac{\partial \Psi}{\partial \underline{\varepsilon}}\underline{\mathring{\varepsilon}} - \frac{\partial \Psi}{\partial \underline{\alpha}}\underline{\mathring{\alpha}} - \frac{\partial \Psi}{\partial \underline{V}}\underline{\dot{V}} - \left(\eta + \frac{\partial \Psi}{\partial \theta}\right)\dot{\theta} - \frac{1}{\rho_0 \theta}\mathbf{q}_0 \cdot \mathrm{Grad}\theta \geq 0, \tag{10}$$

where the total time derivative in Eq. (7) for microscopic quantities $\underline{\varepsilon}$ and $\underline{\alpha}$ dependent on the volume fractions $\underline{V}$. Moreover, the thermodynamic forces $\overline{\kappa} = [\kappa_0, \kappa_1, \ldots, \kappa_{n_c}]^T$, $\underline{\overline{\alpha}} = [\alpha_0, \alpha_1, \ldots, \alpha_{n_c}]^T$ and $\underline{P} = [P_0, P_1, \ldots, P_{n_c}]^T$ are defined, which in summary renders a set of constitutive relations as

$$1. \quad \overline{\mathbf{M}} = \rho_0 2\overline{\mathbf{C}}_e \cdot \frac{\partial \Psi}{\partial \overline{\mathbf{C}}_e}, \qquad 2. \quad \overline{\kappa} = \rho_0 \frac{\partial \Psi}{\partial \underline{\varepsilon}}, \qquad 3. \quad \underline{\overline{\zeta}} = \rho_0 \frac{\partial \Psi}{\partial \underline{\alpha}}, \qquad 4. \quad \underline{P} = \rho_0 \frac{\partial \Psi}{\partial \underline{V}}, \tag{11}$$

As a modification to [2], the thermodynamic forces are obtained within a thermodynamic context. Accounting for the constitutive relations (10) and (11) the following inequalities are obtained

$$1. \quad \mathcal{D}^i = \overline{\mathbf{M}} : \overline{\mathbf{L}}_i - \overline{\kappa}\cdot\underline{\mathring{\varepsilon}} - \underline{\overline{\zeta}}\cdot\underline{\mathring{\alpha}} \geq 0, \qquad 2. \quad \mathcal{D}^V = -\underline{P}\underline{\dot{V}} \geq 0, \qquad 3. \quad \mathcal{D}^\theta = -\frac{1}{\theta}\mathbf{q}_0 \cdot \mathrm{Grad}\theta \geq 0. \tag{12}$$

where $\mathcal{D}^i$ represents the dissipation due to dislocation evolution, $\mathcal{D}^V$ represents the dissipation due to volume fraction evolution whilst the term $\mathcal{D}^\theta$ represents dissipation due to thermal evolution. The inequalities Eq. (12.1), Eq. (12.2) and Eq. (12.3) sufficiently validate the Clausius-Duhem inequality Eq. (9), thus proving thermodynamic consistency. For a more in-depth derivation of the validity of Eqs. (12) the authors are referred to [7].

3 PROTOTYPE MODEL

Concrete proposals are made for the model introduced in Section 2, by specifying the Helmholtz energy as well as the evolution of internal variables.

3.1 Helmholtz energy and thermodynamic forces

The Helmholtz energy represents the energy storage caused by small reversible deformations in the crystal lattice and inelastic deformations. Additionally, storage mechanisms, such as dislocation density and energy changes from interfacial effects are included in the Helmholtz energy. The Helmholtz energy

is assumed as the thermodynamic potential

$$
\begin{aligned}
&1.\quad \Psi = \Psi^e[\overline{\mathbf{C}}_e,\theta] + \Psi^\theta[\theta] + \Psi^p[\underline{\varepsilon},\underline{\alpha},\underline{V},\theta], \qquad \text{where}\\
&2.\quad \Psi^e = \frac{1}{2\rho_0}K[\theta](\ln \mathbf{J}_e)^2 + \frac{G[\theta]}{4\rho_0}\left(\mathrm{tr}\left[\ln\hat{\mathbf{C}}_e\right]^2\right) - \frac{3K[\theta]}{\rho_0}\alpha_\theta[\theta]\Delta\theta \ln \mathbf{J}_e,\\
&3.\quad \Psi^\theta = \frac{1}{\rho_0}\int_{\theta_0}^{\theta} c_d[\overline{\theta}]d\overline{\theta} - \frac{\theta}{\rho_0}\int_{\theta_0}^{\theta}\frac{c_d[\overline{\theta}]}{\overline{\theta}}d\overline{\theta}\\
&4.\quad \Psi^p = \frac{G[\theta]}{2\rho_0}\sum_{i=0}^{n_c} V_i c_\varepsilon \varepsilon_i^2 + \frac{G[\theta]}{2\rho_0}\sum_{i=0}^{n_c} V_i c_\alpha \alpha_i^2,
\end{aligned}
\tag{13}
$$

In Eq. (13.1) $\hat{\mathbf{C}}_e$ represents the isochoric elastic strains, ε_i are the lattice strains and α_i are the lattice curvatures.

The thermodynamic forces proposed in Section 2 are specified below. The stress like variables are obtained as

$$
\begin{aligned}
&1.\quad \overline{\kappa}_i = \rho_0\frac{\partial\Psi}{\partial\varepsilon_i} = V_i\kappa_i, \qquad \text{where} \qquad \kappa_i = G[\theta]c_\varepsilon\varepsilon_i,\\
&2.\quad \overline{\zeta}_i = \rho_0\frac{\partial\Psi}{\partial\alpha_i} = V_i\zeta_i, \qquad \text{where} \qquad \zeta_i = G[\theta]c_\alpha\alpha_i,\\
&3.\quad P_i = \rho_0\frac{\partial\Psi}{\partial V_i} = \frac{G[\theta]}{2}\left(c_\varepsilon\varepsilon_i^2 + c_\alpha\alpha_i^2\right) = \frac{1}{2G[\theta]}\left(\frac{\kappa_i^2}{c_\varepsilon} + \frac{\zeta_i^2}{c_\alpha}\right), \qquad i = 0,\ldots,n_c
\end{aligned}
\tag{14}
$$

The thermodynamic forces $\overline{\kappa_i}$ and $\overline{\zeta_i}$ are stress like internal variables conjugate to ε_i and α_i obtained with thermodynamic arguments, in contrast to [2]. The thermodynamic forces P_i are the driving forces for boundary motion sweeping through unrecrystallized material and removing the dislocation density, see e.g. [1].

3.2 Evolution equations for viscoplasticity and recrystallization variables

The evolution equations for viscoplasticity incorporating dynamic recrystallization are specified as

$$
\begin{aligned}
&1.\quad \overline{\mathbf{L}}_i = \overline{\mathbf{L}}_i[\underline{Z}], \qquad 2.\quad \mathring{\underline{\varepsilon}} = \mathring{\underline{\varepsilon}}[\underline{Z}], \qquad 3.\quad \mathring{\underline{\alpha}} = \mathring{\underline{\alpha}}[\underline{Z}], \qquad 4.\quad \dot{\underline{V}} = \dot{\underline{V}}[\underline{Z}], \qquad \text{where}\\
&5.\quad \underline{Z} = [\overline{\mathbf{M}}_C, \overline{\kappa}, \overline{\underline{\zeta}}, \underline{\varepsilon}, \underline{\alpha}, \underline{V}, \underline{P}, \theta]
\end{aligned}
\tag{15}
$$

formulated with the generalized vector $\underline{Z}$, including the Mandel stress tensor $\overline{\mathbf{M}}_C$, the microscopic stresses $\overline{\underline{\kappa}}$ and $\overline{\underline{\zeta}}$ as well as the driving force $\underline{P}$ written in terms of their respective internal variables $\overline{\mathbf{L}}_i$, $\mathring{\underline{\varepsilon}}$, $\mathring{\underline{\alpha}}$ and $\dot{\underline{V}}$.

The flow rule for the viscoplastic part of the velocity gradient $\overline{\mathbf{L}}_i$ in intermediate configuration in

Eq. (4) is obtained as

$$\begin{aligned}
&1.\quad \overline{\mathbf{L}}_i = \dot{\lambda}\sqrt{\frac{3}{2}}\overline{\mathbf{N}}^T, \qquad \text{where}\\
&2.\quad \dot{\lambda} = f[\theta]\left(\sinh\left\langle\frac{\Phi}{Y[\theta]+Q}\right\rangle\right)^{n[\theta]},\\
&3.\quad \Phi = \sigma_v - (Y[\theta]+Q),\\
&4.\quad \sigma_v = \sqrt{\frac{3}{2}}||\overline{\mathbf{M}}_C||,\\
&5.\quad \overline{\mathbf{N}} = \frac{\overline{\mathbf{M}}_C^{dev}}{||\overline{\mathbf{M}}_C^{dev}||},
\end{aligned} \tag{16}$$

where the temperature dependent scalar variables are defined as

$$1.\quad f[\theta] = c_1\exp\left(-\frac{c_2}{\theta}\right), \qquad 2.\quad n[\theta] = c_3 + \frac{c_4}{\theta}, \qquad 3.\quad Y[\theta] = c_5 G[\theta], \tag{17}$$

and where $G[\theta]$ is the shear modulus and c_i, $i = 1,\dots,5$ are material parameters. Each recrystallized volume fraction V_i is deformed with the same plastic rate $\dot{\lambda}$ in Eq. (16.2) based on the following assumptions

$$1.\quad \hat{\lambda} = \frac{\partial\lambda}{\partial\underline{V}}\underline{\dot{V}} = 0 \qquad \Longrightarrow \qquad 2.\quad \mathring{\lambda} = \dot{\lambda}, \qquad \text{where} \qquad \dot{\lambda} = \sqrt{\frac{2}{3}\overline{\mathbf{L}}_i : \overline{\mathbf{L}}_i} = \dot{e}_v \geq 0. \tag{18}$$

The macroscopic flow stress Q, introduced in Eq. (16), is derived as

$$Q := \sum_{i=0}^{n_c}\left[\frac{b^*}{2}\left(\overline{\kappa}_i k_1 k_3 + \frac{k_1 c_\varepsilon}{c_\alpha}\overline{\zeta}_i\right) + \overline{\zeta}_i h_\zeta\left(\frac{\overline{\zeta}_i}{G[\theta]}\right)^{1-1/r}\frac{1}{c_\alpha}\right], \tag{19}$$

where both microstresses $\overline{\kappa}_i$ and $\overline{\zeta}$ contribute to the macroscopic flow stress Q.

Following [2], during dynamic recrystallization in polycrystalline materials the microscopic quantities are three-fold. Firstly, during the plastic deformation of polycrystalline materials, the grains rotate and adjust themselves towards loading direction. This is expressed by the generation of geometrically necessary dislocations, resulting in lattice curvature. The geometrically necessary dislocations L_{gi}^{-1} are assumed to evolve as following

$$1.\quad \overline{\mathring{L}_{gi}^{-1}} = f_i^g\,\mathring{\lambda} = f_i^g\,\dot{\lambda} \geq 0, \qquad \text{where} \qquad 2.\quad f_i^g = c_{Lg}\left(L_{gi}^{-1}\right)^{1-1/r}, \tag{20}$$

and where c_{Lg} and r are material parameters. With the inverse of the average spacing L_{gi} the evolution of the lattice curvature α_i is introduced with

$$1.\quad \mathring{\alpha}_i = \frac{b^* k_2}{k_1}\overline{\mathring{L}_{gi}^{-1}} = f_i^\alpha\dot{\lambda}, \qquad \text{where} \qquad 2.\quad f_i^\alpha = \frac{b^* k_2}{k_1}f_i^g, \tag{21}$$

where k_1 as well as k_2 are material parameters and b^* is the magnitude of the burgers vector. Following the derivations in [2] this renders the misorientation variable ζ_i as

$$\zeta_i = G[\theta]c_\alpha\frac{b^* k_2}{k_1}L_{gi}^{-1}, \tag{22}$$

with $G[\theta]$ being the shear modulus and c_α being a material parameter.

Secondly, with progressing deformation statistically stored dislocations occur, which in contrast to the geometrically necessary dislocations are divided into generation and annihilation. The evolution equations for the statistically stored dislocations density read as

$$\begin{aligned} &1.\quad \mathring{\rho}_i = f_i^\rho \mathring{\lambda} = f_i^\rho \dot{\lambda}, \qquad \text{where} \qquad 2.\quad f_i^\rho = k_1 L_{si}^{-1} + k_2 L_{gi}^{-1} - R_d[\theta]\rho_i, \\ &3.\quad L_{si}^{-1} = k_3\sqrt{\rho_i}, \qquad 4.\quad R_d[\theta] = c_6 \exp\left(-\frac{c_7}{\theta}\right), \end{aligned} \tag{23}$$

With the dislocation density ρ_i at hand the evolution of lattice s train ε_i for each cycle is specified to

$$1.\quad \mathring{\varepsilon}_i = f_i^\varepsilon \dot{\lambda}, \qquad \text{where} \qquad 2.\quad f_i^\varepsilon = \frac{b^*}{2\sqrt{\rho_i}} f_i^\rho. \tag{24}$$

The corresponding micro stress is to be interpreted as the hardening variable and reads as

$$\kappa_i = c_\varepsilon G[\theta] b^* \sqrt{\rho_i}. \tag{25}$$

Thirdly, as stated in section 2.1 dynamic recrystallization occurs in cycles described by recrystallized fractions X_i. According to [2] the recrystallized fraction is written as follows:

$$\begin{aligned} &1.\quad \dot{X}_i = A_i G_i f[X_{i-1}], \qquad 2.\quad A_i = X_{i-1}\left(\frac{X_i}{X_{i-1}}\right)^a \left(\frac{1-X_i}{X_{i-1}}\right)^b, \qquad 3.\quad G_i = M_i P_i, \\ &4.\quad M_i[\zeta_i] = M_0 \exp\left(-\frac{Q_g}{R\theta}\right)\left(1-\exp\left(-B\left(\frac{\zeta_i}{G[\theta]}\right)^m\right)\right), \\ &5.\quad P_i[\varepsilon_i,\alpha_i] = \frac{1}{2G[\theta]}\left(\frac{\kappa_i^2}{c_\varepsilon} + \frac{\zeta_i^2}{c_\alpha}\right), \qquad 6.\quad 1 + c(1-X_{i-1}), \end{aligned} \tag{26}$$

where A_i is the interfacial area dividing recrystallized and unrecrystallized material. The interfacial area sweeps through the unrecrystallized area with the interface velocity G_i related to the boundary mobility M_i. Finally, M_0, Q_q, R, B and M are material parameters.

4 SIMULATION EXAMPLES

The objective of the numerical examples is the validation of the proposed model based on the experimental data for OFHC copper provided in [9]. The material parameters in Table 1 are obtained solving the inverse problem during parameter identification. Since the same data is used in [2], comparison between the numerical results of [2] and the proposed model can be drawn.

Table 1: Material parameters for strain type formulation for OFHC copper

Function	Parameter	Value	Unit	Function	Parameter	Value	Unit
	b^*	0.250E+00	-	$Q_i[T]$	B	1.360E+09	-
$f[\theta]$	c_1	2.135E−01	1/s		m	2.802E+00	-
	c_2	1.326E+00	K		c_κ	8.657E+11	K/MPa s
$n[\theta]$	c_3	1.640E+01	-		c_ζ	6.017E+11	K/MPa s
$Y[\theta]$	c_5	8.797E−04	-	$g_i[\theta]$	a	2.704E−01	-
$H[\theta]$	c_8	1.318E−02	-		b	1.142E+00	-
$R_d[\theta]$	c_6	8.090E+00	-		c	2.579E+01	-
	c_7	3.282E+02	K		k_1	0.720E+00	-
	h_ζ	2.307E−05	1/s		k_2	1.003E+00	-
	r	6.481E−01	-		k_3	1.083E+01	-
$R_i[\theta]$	c_T	1.831E+04	K				

The experimental data for OFHC copper as well as the results of the proposed equations for the case of uniaxial loading is presented in Figure 2. Here, σ is the non-vanishing part of the Cauchy stress tensor and ε is the axial component of the Eulerian strain tensor. From Figure 2 characteristic phenomena for dynamic recrystallization become apparent.

- Recrystallization does not occur at room temperature, thus the true stress at $\theta = 25\,^\circ\mathrm{C}$ does not show softening.
- Depending on temperature and strain rate, single as well as multi-peak recrystallization may occur. Especially low strain rate exhibit the cyclic hardening and recovering.
- OFHC copper shows a high temperature and strain rate dependence, which can be captured by the model.

To discuss the characteristic behavior of dynamic recrystallization, the load case with constant temperature $\theta = 337\,^\circ\mathrm{C}$ and uniaxial strain rate $\dot{\varepsilon} = 0.0004\,/\mathrm{s}$ is presented in more detail. The strain type microscopic quantities are presented in Figure 3 and Figure 4 for six concurrent recrystallization cycles. Figure 3a shows the average spacing between geometrically necessary dislocations L_{gi}^{-1} and Figure 3b shows the statistically stored dislocation density ρ_i. The evolution of lattice curvature α_i as well as lattice strain ε_i is presented in Figure 4a and 4b, respectively. In Figure 5 the evolution of stress type variables is compared to the numerical results of [2]. The results of the proposed mode are presented with solid lines, while results of [2] use dashed lines. The micro stresses $\overline{\zeta}_i$ describing the misorientation of the grains is shown in Figure 5a, whereas the micro stresses $\overline{\kappa}_i$ describing the hardening and recovering is presented in Figure 5b. Due to increasing strain the sub grain spacing decreases and the misorientation $\overline{\zeta}_i$ variable can be seen to increase. The rate of the isotropic hardening variable $\overline{\kappa}_i$ declines continually while never reaching a steady-state value. At the onset, the isotropic hardening variable $\overline{\kappa}_2$ increases and causes hardening and decreases as more recrystallized material is added to the volume fraction. With increasing volume fraction V_2 hardening starts to overtake softening and the isotropic hardening variable increases again.

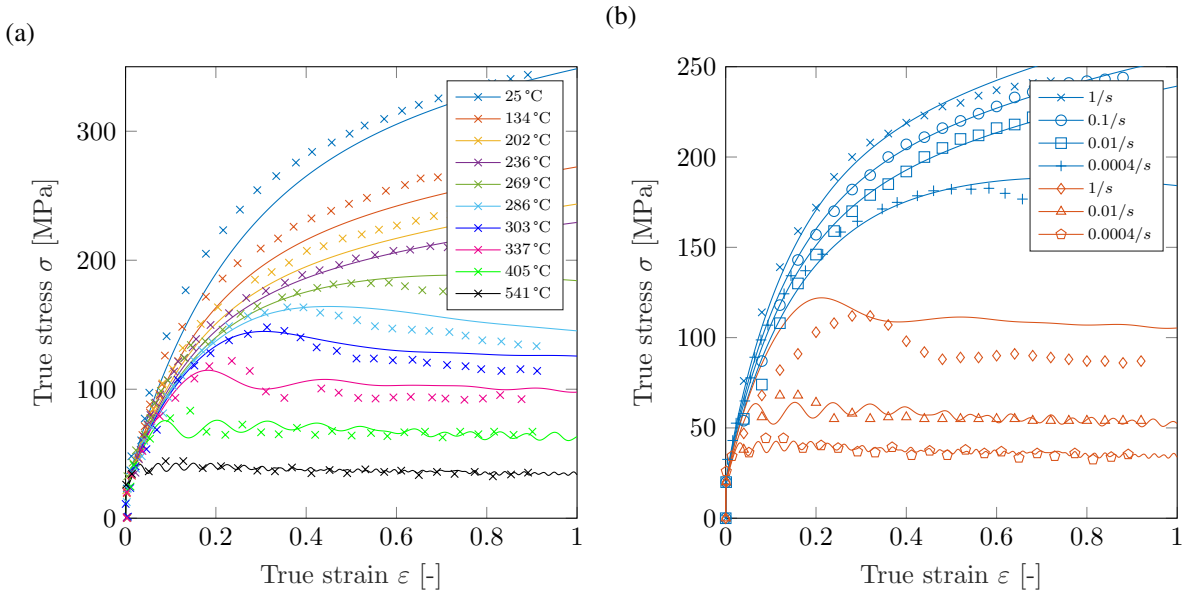

Figure 2: True stresses σ at various temperatures and strain rates, experimental data by [9] (markers), results of parameter identification for present model (solid lines), (a) constant strain rate $\dot{\varepsilon} = 0.0004/\mathrm{s}$, (b) constant temperatures $\theta = 269\,°\mathrm{C}$ (blue) and $\theta = 541\,°\mathrm{C}$ (red).

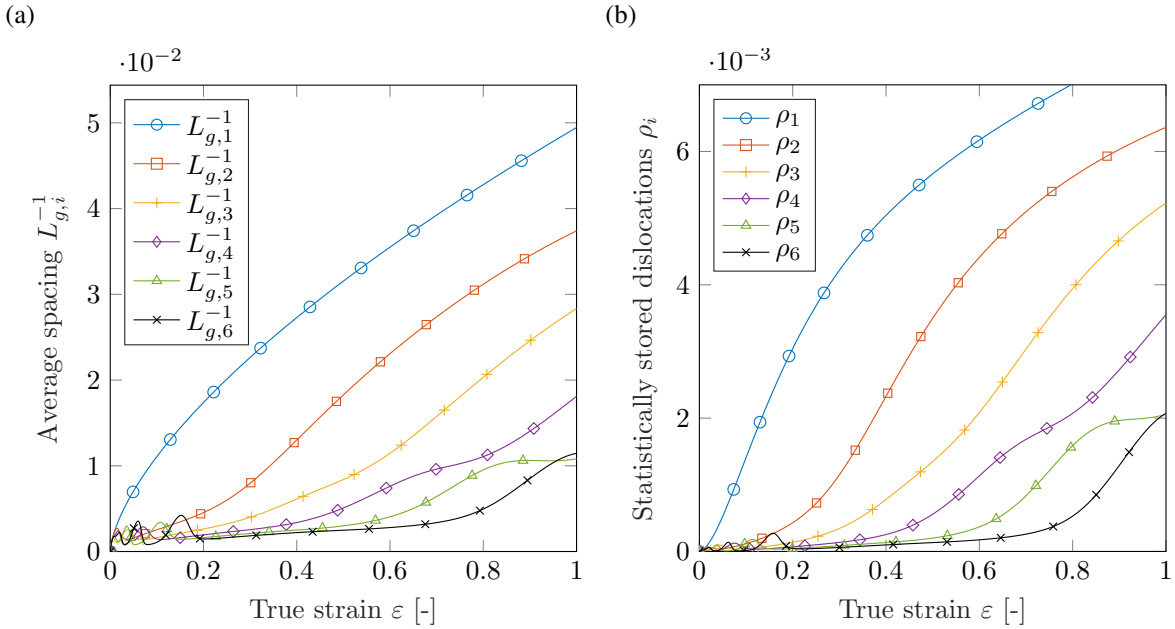

Figure 3: Strain type variables: (a) Average spacing between geometrically necessary dislocation $L_{g,i}^{-1}$, (b) statistically stored dislocation density ρ_i.

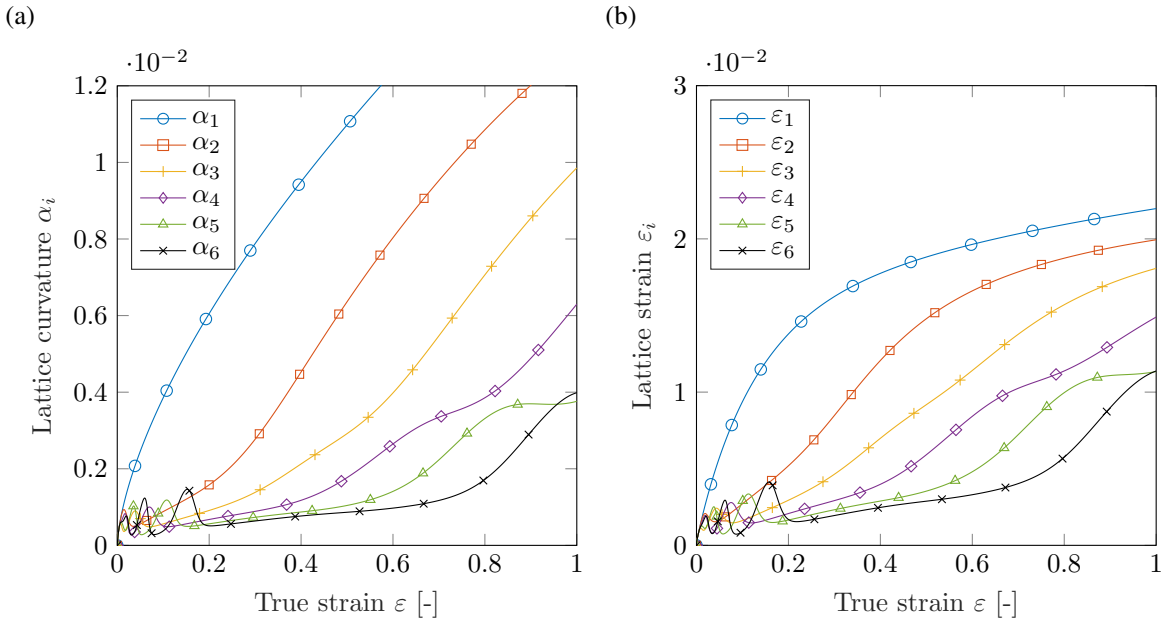

Figure 4: Strain type variables: (a) Lattice curvature α_i, (b) Lattice strain ε_i.

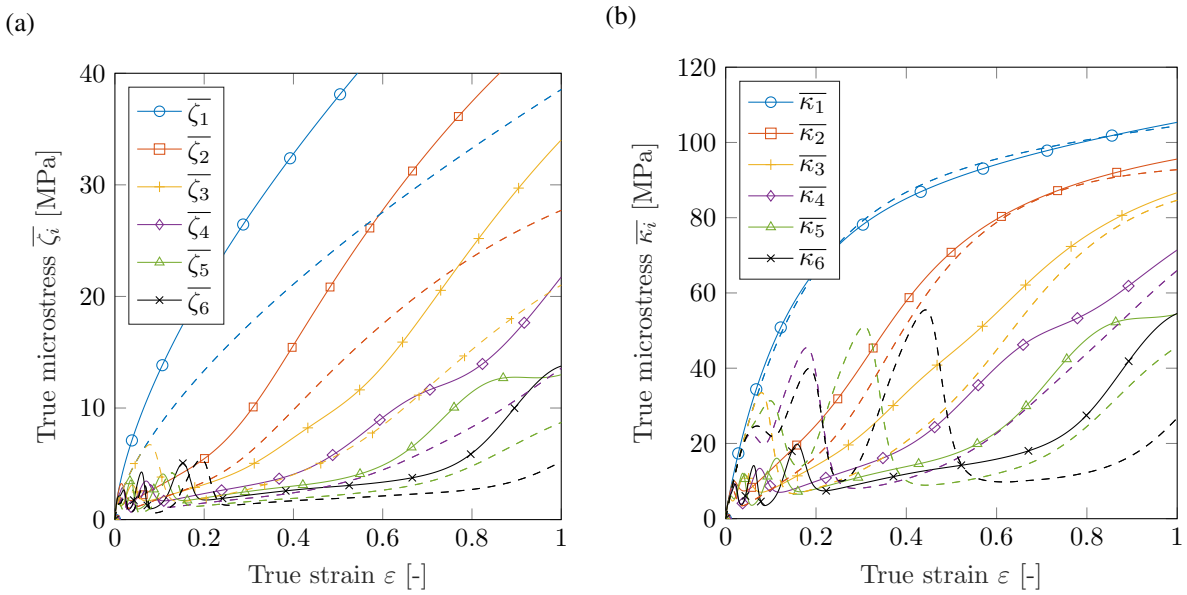

Figure 5: Stress type variables: Comparison between present model (solid lines) and the original model [2] (dashed lines): (a) Misorientation variable $\overline{\zeta_i}$, (b) Isotropic hardening variable $\overline{\kappa_i}$.

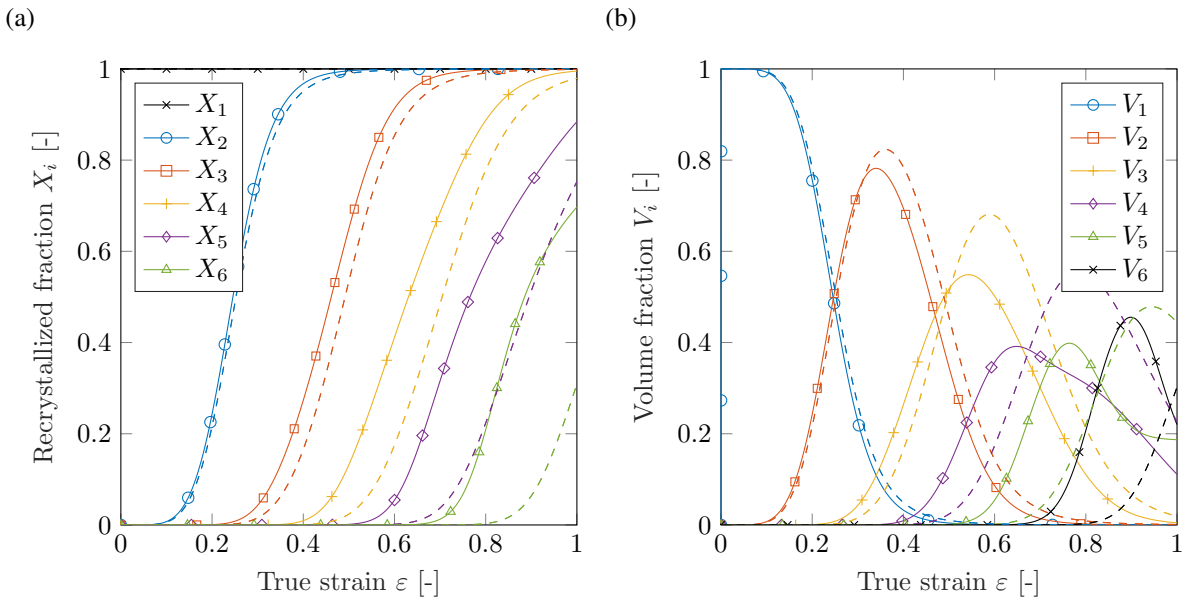

Figure 6: Recrystallization kinetics: Comparison between present model (solid lines) and the original model [2] (dashed lines): (a) Recrystallized fraction X_i, (b) Recrystallized volume fraction V_i.

5 CONCLUSIONS

A thermodynamic framework for viscoplasticity coupled to dynamic recrystallization was developed, as modification to the proposal in [2]. The recrystallized volume fractions are incorporated in the Helmholtz energy, thus defining the recrystallization quantities dependent on time for varying recrystallization quantities. As a result the evolution equations are split into an explicit and convective part. By distinguishing between true micros tresses in the recrystallized phase and nominal micro stresses in the complete phase, similar evolution equations for the recrystallization quantities in [2] were derived.

The capabilities of the model have been presented in numerical examples. During parameter identification material parameters were identified and subsequent numerical results are in good agreement with the experimental data presented in [9] and the results of the original model in [2].

REFERENCES

[1] Gottstein, G. *Physikalische Grundlagen der Materialkunde.* Springer-Verlag Berlin Heidelberg, Vol. III. (2007).

[2] Brown, A. A. and Bammann, D. J. Validation of a model for static and dynamic recrystallization in metals. *International Journal of Plasticity.* (2012) **32-33**.

[3] Bammann, D.J. Modeling Temperature and Strain Rate Dependent Large Deformations of Metals. *Applied Mechanics Reviews.* (1990) **43**:312–319.

[4] Bammann, D. Prantil, V. and Lathrop, J. A model of phase transformation plasticity. *Technical Report. Sandia National Labs.* (1995)

[5] Bammann, D. Prantil, V. and Lathrop, J. A plasticity model for materials undergoing phase transformations. *Simulation of Materials Processing: Theory, Methods and Applications.* (1995)

95:219–224.

[6] Bammann, D. Chiesa M. Johnson, G. Modeling large deformation and failure in manufacturing processes. *Theoretical and Applied Mechanics.* (1996) **9**:359–376.

[7] Mahnken, R. and Westermann, H. A non-equilibrium thermodynamic framework for viscoplasticity incorporating dynamic recrystallization at large strains. *In revision.* (2021)

[8] Mahnken, R. Wolff, M. and Cheng, C. A multi-mechanism model for cutting simulations combining visco-plastic asymmetry and phase transformation. *International Journal of Solids and Structures.* (2013) **50**:3045–3066.

[9] Tanner, A.B. and McDowell, D.L. Deformation, temperature and strain rate sequence experiments on ofhc cu. *International Journal of Plasticity.* (1999) **15**: 375–399.